Numerical analysis of GFRP-reinforced concrete elements subjected to fire

Carolina Veríssimo Churro Instituto Superior Técnico

Abstract

Used in the building industry since the 1980's, fibre reinforced polymers (FRP) have numerous advantages when compared to traditional steel reinforcement in reinforced concrete elements. However, there are still some concerns about the use of this material in current buildings due to its behaviour under high temperatures. Effectively, the mechanical properties and the bond between the rebars and the concrete are strongly affected by high temperatures, especially when the glass transition temperature (T_g) of the matrix is approached or exceeded. In the present paper, numerical studies about the fire behaviour of glass fibre-reinforced polymer (GFRP) reinforced concrete (RC) slab strips are presented. The numerical studies were performed on steel- and GFRP-RC slab strips subjected to the ISO 834 standard curve. Accordingly, five slab strips were modelled to evaluate the influence of the concrete cover (2.5 and 3.5 cm) and of the existence of lap splices directly exposed to heat with two different overlap lengths (30 and 60 cm). The numerical models also included two different approaches regarding the bond between the rebars and the concrete: (i) a perfect and temperature independent bond; and (ii) a bond-slip relation available in the literature, which takes into account the degradation of the bond properties with the increasing temperature. The numerical investigation was divided in three different phases: (i) a mechanical analysis, in which the slabs were subjected to a mechanical load at ambient temperature; (ii) a thermal analysis, in which the ISO 834 standard curve was applied to the slabs, and (iii) a thermo-mechanical analysis, in which the fire behaviour of the slabs was assessed, by combining a mechanical load with the temperatures obtained from the thermal analysis. The numerical results obtained, in general, were in a reasonable agreement with the corresponding experimental data; particularly, the results obtained in the thermo-mechanical analysis confirm that (i) GFRF-RC slabs with continuous reinforcement exhibit substantial fire resistance (about 120 minutes), provided that the anchorage zones of the rebars remain relatively cold, (ii) the presence of lap splices directly exposed to heat significantly decreases such fire resistance to about 20 minutes. The consideration of a temperature-dependent bond is more significant when applied to GFRP-RC slabs with lap spliced rebars, precisely due to the slippage failure of the rebars. The fire resistance estimated from the models was generally higher than that measured in the tests; it is likely that the bond-slip relations that were used to simulate the bond between the rebars and the concrete may have slightly overestimated the bond performance.

Keywords: glass fibre reinforced polymers (GFRP), reinforced concrete, numerical study, fire behaviour, bond.

1. Introduction and state of the art

Fibre-reinforced polymer (FRP) materials have been increasingly used in civil engineering applications since the 1980's when the means of production became more efficient and economic. Since the fibres present a high tensile resistance and the polymeric matrix protects them from moisture and alkaline salts, FRP's present a good alternative over traditional steel rebars when used as reinforcement of concrete elements subjected to aggressive environments [1]. However, with increasing temperature, especially when the glass transition temperature (T_g) of the matrix is approached or exceeded, their mechanical properties and the bond between the rebars and the concrete are strongly affected and this has been preventing the widespread use of these materials in buildings, where fire is a design action. Even though there are some studies available in the literature about this phenomenon, this issue is still not well understood and further studies are required to fully understand it. Particularly, the few numerical studies available in the literature often include very simple approaches to complex issues, such as the reduction of the bond stresses between the rebars and the concrete with the increasing temperatures or the heat transfer through the elements.

Rafi and Nadjai [2,3] carried out numerical studies in simply supported carbon FRP (CFRP) and hybrid (steel-CFRP) reinforced concrete beams subjected to elevated temperatures. Even though the results obtained cannot be inferred as valid to GFRP reinforced concrete beams, the geometry and setup of the tested elements is similar to the one used in the present work. Experimental studies were carried out in order to evaluate temperature-dependent strength and stiffness properties of the CFRP [4], and such proposed constitutive laws were later used in the numerical models. A three-dimensional solid brick element with 20 nodes was used in the finite elements analysis due to its satisfactory performance for heat transfer analysis, adequate accuracy in terms of displacement and internal forces, numerical robustness. Given the geometric

and load symmetry in the longitudinal and transverse directions, only one quarter of the beam was modelled with the commercial software Diana. The authors used a typical mesh (with a maximum size of 40 mm) with a finer discretization in the zones with steeper thermal gradients. The concrete modulus of elasticity was calculated from an expression available in [5]; the temperature-dependent compressive and tensile resistances, the specific heat and the thermal conductivity of the concrete were obtained from [6] and the thermal expansion coefficients were obtained from expressions proposed by [3]. Due to the lack of information about the subject, the bond between the rebars and the concrete was considered perfect and temperature-independent. In the thermal analysis the authors used small time steps (1 min) to obtain the nodal temperatures with a 1×10^{-6} and 5×10^{-2} tolerance, respectively, in the temperatures and displacements. The number of iterations for each time step was limited to 5 in order to assure a steep convergence. The authors concluded that the results obtained showed good agreement with the results obtained experimentally, with differences of about 10% for the mid-span displacements and fire resistances.

Yu and Kodur [7,8] adapted a model originally developed for steel reinforced concrete beams in order to assess the effects of: (i) three different types of rebars (steel, carbon FRP and glass FRP) and (ii) the existence of exterior fire protection. The thermal and mechanical effects were separated to facilitate the analysis. The bond properties between the different rebars and the concrete were modelled indirectly by adding a strain resulting from the slip to the total strain of the element; thus, for each time step, the shear stress on the surface between the rebars and the concrete, τ, was given by:

$$\tau.\left(\pi.d_{bar}.L_{eff}\right) = \sigma_{FRP}.\frac{\pi.d_{bar}^2}{4} \quad (1)$$

where d_{bar} is the diameter of the rebars, L_{eff} is the effective length of the anchorage and σ_{FRP} is the tensile stress on the FRP rebars. The slip strain was then calculated, for each time step, by:

$$\varepsilon_{slip} = \begin{cases} \tau/E_{bond}, & \tau > f_{bond} \\ 0, & \tau \leq f_{bond} \end{cases} \quad (2)$$

The authors concluded that concrete beams reinforced with GFRP present lower fire resistance than steel- or CFRP-reinforced concrete beams and that an appropriate exterior fire protection can enhance significantly the fire resistance; particularly, a fire protection with 24 mm of thickness on the bottom of the beam and extended to 150 mm of depth on the two sides of the beam can increase the fire resistance from 70 minutes to 180 minutes. The authors also conducted a parametric analysis to evaluate the effect of: (i) the concrete cover, (ii) the presence of axial restraints, and (iii) the consideration of more moderate fire scenarios. The authors concluded that increasing the concrete cover enhances the fire resistance, even if not significantly. The presence of an axial restraint also increases the fire resistance by about 5-30 minutes due to the effect of an arch action mechanism, when compared to simply supported beams. Finally, the consideration of a more moderate fire scenario increases the fire resistance by reducing the temperatures in the rebars.

Nigro *et al.* [9] conducted a numerical program on GFRP reinforced concrete slabs through the commercial software ABAQUS. Thermal and mechanical analysis were separated to facilitate the analysis and a 3D solid brick element with 8 nodes was used in the finite elements analysis. The bond between the rebars and the concrete was simplified and considered non-existent on the zones subjected to the elevated temperatures and perfect on the relatively cold anchorages, near the support. The authors obtained very good agreements in terms of thermal fields and reasonable agreements in terms of mechanical simulations between the numerical and experimental results, even though they considered a simpler approach to the bond behaviour on the rebar-concrete interface.

Apart from the above mentioned numerical studies, there are no data available in the literature regarding the numerical analysis of FRP reinforced concrete elements. Moreover, according to the author's best knowledge, there are still no numerical studies in the literature exploring the complex effects of considering a temperature-dependent bond-slip relation on the rebar-concrete interface on the mechanical response of concrete elements. Therefore, further numerical investigations on the mechanical response of GFRP reinforced concrete elements subjected to fire are necessary. In this context, this paper presents the results of a numerical investigation, developed within the author's master dissertation, conducted on five different slab strips, tested recently at IST for the Fire-Composite project [10]. The numerical studies were performed on steel and GFRP reinforced concrete slab strips subjected to the ISO 834 standard curve. Accordingly, five slab strips were modelled to evaluate the influence of the concrete cover (2.5 and 3.5 cm) and the existence of lap splices directly exposed to heat with two different development lengths (30 and 60 cm). The numerical models also included two different approaches regarding the bond between the rebars and the concrete: (i) a perfect temperature independent bond; and (ii) a bond-slip relation available in the

literature, which takes into account the degradation of the bond properties with the increasing temperature. The numerical investigation was divided in three different phases: (i) a mechanical analysis, in which the slabs were subjected to a mechanical load at ambient temperature; (ii) a thermal analysis, in which the ISO 834 standard curve was applied to the slabs and (iii) a thermo-mechanical analysis, in which the fire behaviour of the slabs was assessed, by combining a mechanical load with the temperatures attained at the thermal analysis.

2. Summary of the experimental study

2.1 Test programme

The experimental campaign conducted at IST comprised a series of tests to assess the properties of the different materials, such as: (i) concrete characterization tests at room temperature at 28 days and 135 days of age, (ii) DMA tests to evaluate the GFRP's glass transition temperature, T_g, and (iii) tensile tests on GFRP rebars at room and elevated temperatures to assess the degradation of the elasticity modulus and of the tensile strength with the increasing temperature. Additionally, the experimental campaign included tests carried out on slabs, namely, flexural tests at room temperature and fire resistance tests.

2.2 Design and materials

As mentioned, five different types of steel and GFRP reinforced concrete slab strips were tested at IST for the Fire-Composite project [10] to evaluate the influence of the concrete cover (2.5 and 3.5 cm) and the existence of lap splices directly exposed to heat with two different development lengths (30 and 60 cm). The slab strips were calculated as simply supported beams with a span between supports of 1.40 m and subjected to two concentrated forces applied at thirds of the span, Figure 1.

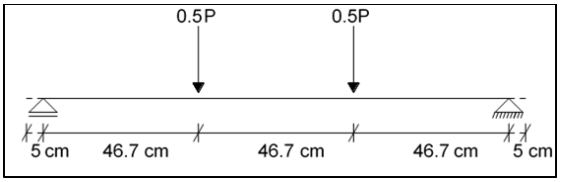

Figure 1 - Simply supported beam model (adapted from [10])

The five tested slab strips presented the same dimensions with length of 1.50 m, width of 0.25 m and thickness of 0.11 m. The slab strips were produced with C25/30 concrete; regarding the reinforcement, the RC slab strip was reinforced with traditional A500 ribbed steel rebars with nominal diameter of 10 mm and the GFRP rebars, supplied by Hughes Brothers (model Aslan100), have 10 mm of diameter and a sand coated finishing with exterior helicoidal fibres. Thermocouples were placed inside the five slab strips (one of each type) used in the fire resistance tests; the position of the thermocouples can be found in Figure 3. As mentioned, in order to determine the properties of the concrete and of the GFRP rebars used in the experimental campaign several tests were conducted; the test results can be found in Table 1 and Table 2.

Table 1 - Concrete characterization test results (adapted from [10])

Property	Concrete age at the time of the tests					
	28 days			135 days		
Compression strength (cubes)	fcm [MPa]	Sn [MPa]	fck [MPa]	fcm [MPa]	Sn [MPa]	fck [MPa]
	31.2	1.1	29.4	53.3	2.1	49.8
Tensile strength	fctm [MPa]			fctm [MPa]		
	2.2			2.8		
Elasticity modulus (estimated from the compression tests)	Ecm [GPa]			Ecm [GPa]		
	31			36.3		

Table 2 - Results of the tensile tests on GFRP rebars (adapted from [10])

Temperature [ºC]	Strength [MPa]	Elasticity Modulus [GPa]
	Average ± STD	Average ± STD
20	1045.0 ± 8.4	48.2 ± 0.8
50	927.5 ± 8.0	47.6 ± 0.1
100	682.4 ± 14.6	44.1 ± 1.2
150	623.2 ± 30.6	45.9 ± 1.3
200	603.7 ± 15.1	45.3 ± 2.2
250	619.3 ± 11.2	43.7 ± 3.6
300	598.2 ± 23.5	41.8 ± 4.1

2.3 Test setup

The slab strips were all produced and tested at IST. Five slab strips were subjected to flexural tests at room temperature in order to assess their mechanical behaviour and failure modes. Each slab was subjected to a monotonic load until failure with small pauses to measure cracking patterns, during which the load was maintained approximately constant. The test setup is similar to the one presented in Figure 1. The loading was stopped at important design values, such as the cracking load and pre-defined percentages of the resistance of the element.

The test setup of the fire resistance tests is shown in Figure 2. The slab strips were placed in a furnace and subjected to the ISO 834 standard fire curve, while being simultaneously mechanically loaded through the dead load of two concrete blocks attached to a distribution beam. The results of both tests are presented in section 4, alongside the numerical results in order to establish a direct comparison between the experimental and numerical results regarding mid-span displacements, failure loads and modes, nodal temperatures and fire resistance.

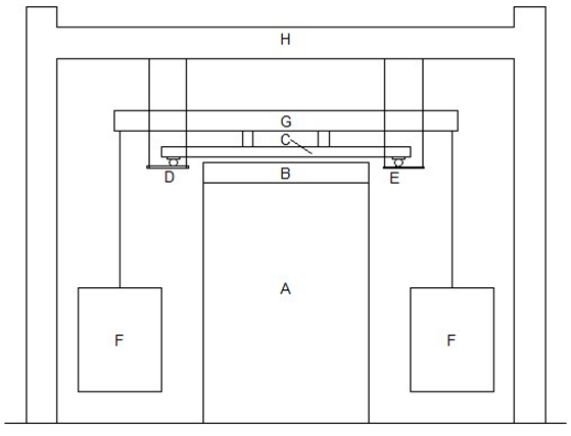

Figure 2 - Fire resistance test setup: A - furnace, B – thermal insulation system, C – slab strip, D – movable support, E – hinged support, F – concrete blocks, G – distribution beam e H – reaction frame (adapted from [10])

3. Numerical programme

The numerical programme was developed in order to assess the behaviour of steel and GFRP reinforced concrete slab strips subjected to elevated temperatures and to evaluate the influence of concrete cover, type of reinforcement and existence and length of lap splices located at mid-span. Additionally, the numerical models also included two different approaches to the problem of the bond between rebars and concrete: (i) a perfect temperature-independent bond; and (ii) a temperature dependent bond slip relation, available in the literature. As mentioned, the numerical programme was divided into three phases, each corresponding to a different analysis: (i) a mechanical analysis, in which the slabs were subjected to a mechanical load at room temperature to assess mechanical behaviour and failure modes of the different slabs; (ii) a thermal analysis, in which the nodal temperatures were obtained by applying the ISO 834 standard fire curve; and (iii) a thermo-mechanical analysis in which the nodal temperatures attained in the thermal analysis were combined with a mechanical load, to assess the fire resistance behaviour of the slabs.

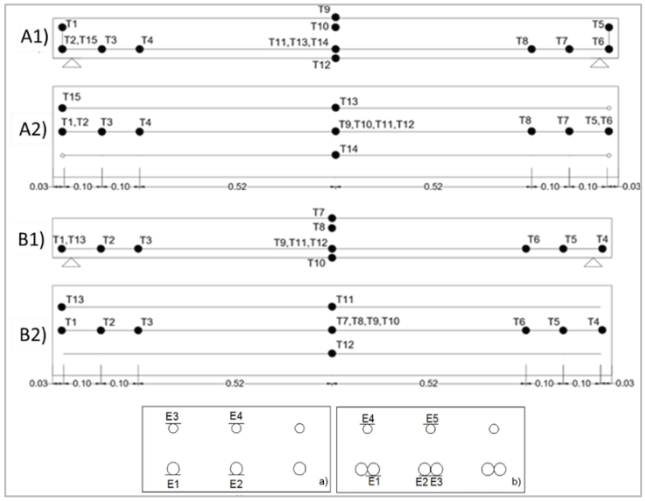

Figure 3 - Location of the thermocouples: A1) RC slab - side, A2) RC slab - plan, B1) GFRP slabs - side, B2) GFRP slabs - plan and position of extensometers (adapted from [10])

3.1 Geometry and element types

The slab strips tested experimentally were modelled with the commercial finite element software ABAQUS. The geometry of the slabs is similar to the one considered in the experimental programme; nonetheless, due to the symmetry in the longitudinal and transverse directions, only one twelfth (0.75 m of length, 0.11 m of thickness and 0.042 m of width) of the slabs reinforced with continuous rebars and one third of the slabs with mid-span lap splices (1.50 m of length, 0.11 m of thickness and 0.084 m of width) was modelled. The position of the rebars was maintained; however, straight steel rebars were used in the numerical models due to the little degradation of the bond properties between steel rebars and concrete elements with increasing temperatures and the limited temperatures measured at the extremity of those rebars. Figure 4 shows the meshes used in the slabs with continuous reinforcement and in the slabs with mid-span lap splices. A three-dimensional hex-type element with 8 nodes was used in the slabs with continuous reinforcement; a three-dimensional wedge-type element with 6 nodes was used in the slabs with lap splices in order to overcome the problem of anti-symmetry in the mid-span lap splices; both elements show satisfactory results in both mechanical and heat transfer analysis. A finer mesh was considered in the zones with steeper thermal gradients and near the rebars, since further accuracy was required in these zones. The models of the slabs with continuous reinforcement were divided in the longitudinal direction into elements with approximately 8.4 mm of size and the section of the rebars was divided (by number) into 6 elements. The models of the slabs with mid-span lap splices, were divided in the longitudinal direction Into elements with approximately 24 mm and the perimeter of the rebars was divided into elements with 4 mm.

3.2 Material and bond properties

The steel of the rebars was modelled as an elastic-plastic with work hardening material in which E_s = 210 GPa, f_y = 535 MPa, f_u = 650 MPa and ν = 0.3. The degradation of the mechanical and thermo-physical properties of steel were considered according to [6]. A concrete damaged plasticity model was used to simulate the mechanical properties of concrete due to its capacity of taking into account the inelastic behaviour of the material and resulting cracking and displacement [11]. The fracture energy was calculated from an expression available in [12] and considered equal to 0.083 N/mm. The temperature dependent thermo-physical properties and the thermal expansion coefficient were calculated according to [6]; the evolution with temperature of the mechanical properties was obtained from [13] (based on [6]). The GFRP mechanical properties up to 300ºC were obtained from [10]; for temperatures between 300ºC and 500ºC, the elastic modulus was obtained from [14]. The reduction of the tensile strength was calibrated to obtain similar failure instants in the numerical models and experimental tests. The thermo-physical properties of GFRP were obtained from [15], who conducted tests in GFRP profiles with a similar fibre percentage. Although the GFRP material has an orthotropic behaviour, the GFRP rebars were modelled as an isotropic material. The thermal expansion coefficient was considered equal to 6×10^{-6} /ºC and constant with the temperature [1].

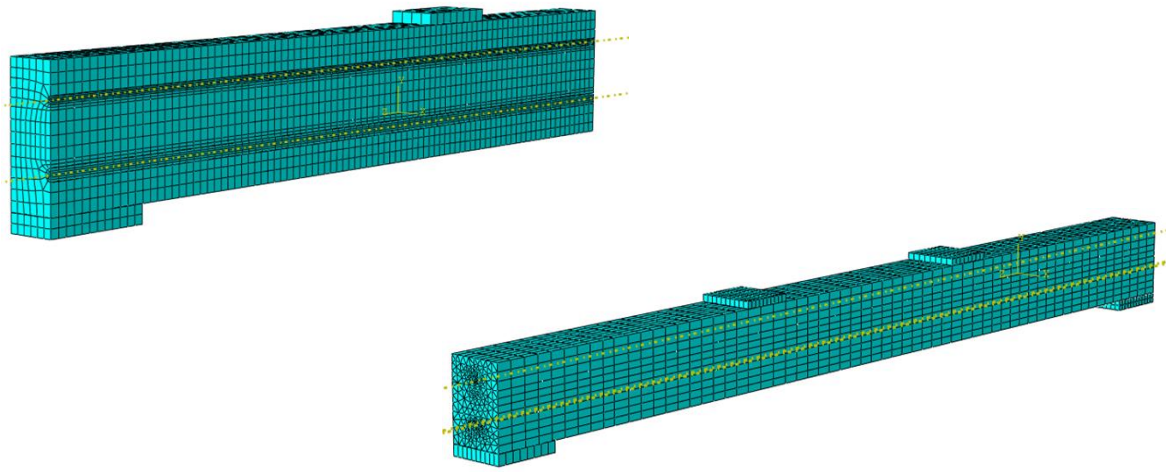

Figure 4 - Geometry and adopted finite elements mesh for the slabs with continuous reinforcement (top) and lap spliced reinforcement (bottom)

As mentioned, two approaches were considered for the bond properties between the rebars and the concrete: (i) a perfect temperature independent bond; and (ii) a temperature dependent bond-slip relation available in the literature [16], in both the mechanical analysis (room temperature) or the thermo-mechanical analysis (fire resistance tests). These bond-slip relations were obtained from pull-out tests conducted at 20ºC, 60ºC, 100ºC and 140ºC; since the bond performance at 140 ºC was already very low, it was considered that for higher temperatures the bond properties would be negligible.

3.3 Boundary and support conditions

The boundary and support conditions were chosen in order to reproduce the conditions of the slabs tested experimentally. Figure 5 represents the boundary conditions considered in the slabs with continuous reinforcement and in the slabs with mid-span lap splices. Both boundary conditions allow the vertical translations of the slab but restraint the rotations. In the thermal analysis, the boundary conditions were chosen in order to reproduce the conditions inside the furnace; thus, radiation and convection surfaces were considered both at the base (in the free span subjected to the fire curve, 1.05 m) and at the top of the slab. The convection coefficient was considered temperature independent and equal to 25 $W/m^2.ºC$, the room temperature was set at 21ºC and the concrete emissivity as 0.7. The temperature around the top and the supported end side(s) was set constant as 21ºC, and convection and radiation heat exchanges were also considered at those boundaries. The support conditions were materialized through the consideration of steel plates, where pinned conditions were applied; the plates guarantee a reaction distribution and were modelled with the same dimensions considered experimentally [10].

3.4 Types of analysis and increments

As mentioned above, in order to facilitate the analysis, the thermal and mechanical effects were separated and the numerical program was divided into three distinct phases. In the mechanical analysis the load was simulated through the consideration of an imposed displacement, with minimum and maximum increments of 1×10^{-15} and 0.01, respectively, through the Newton-Raphson iterative incremental method. It was also specified that consecutive displacements should present differences of less than 10% to avoid non-convergence of the model. The concrete damaged plasticity model considered is incapable of reproducing a shear failure mode due the flexural cracking of the concrete; accordingly, the results of the GFRP reinforced slabs models were only considered until the formation of a shear cracking pattern, which corresponds to the failure of the slab.

A maximum of 7200 seconds (corresponding to a fire exposure of 2 hours) was defined to the thermal analysis. A maximum increment of 60 seconds and a maximum difference for the node temperatures in consecutive increments of 10ºC was also set.

The load applied in the thermo-mechanical analysis was similar to the one considered in the experimental program, corresponding to a percentage of the design load at room temperature for each slab [10]. Just like in the thermal analysis, a fire exposure of 2 hours was considered. The total load was statically applied during the first second of the tests and kept constant for the remaining time. The data was collected based on its level of importance: (i) during the first second the data was fully collected, (ii) between the 10^{th} and the 500^{th} second the data was collected every 10 seconds and (iii) from the 510^{th} second until the end of the simulation the data was collected every 60 seconds. The maximum increment allowed for the algorithm was 10 seconds.

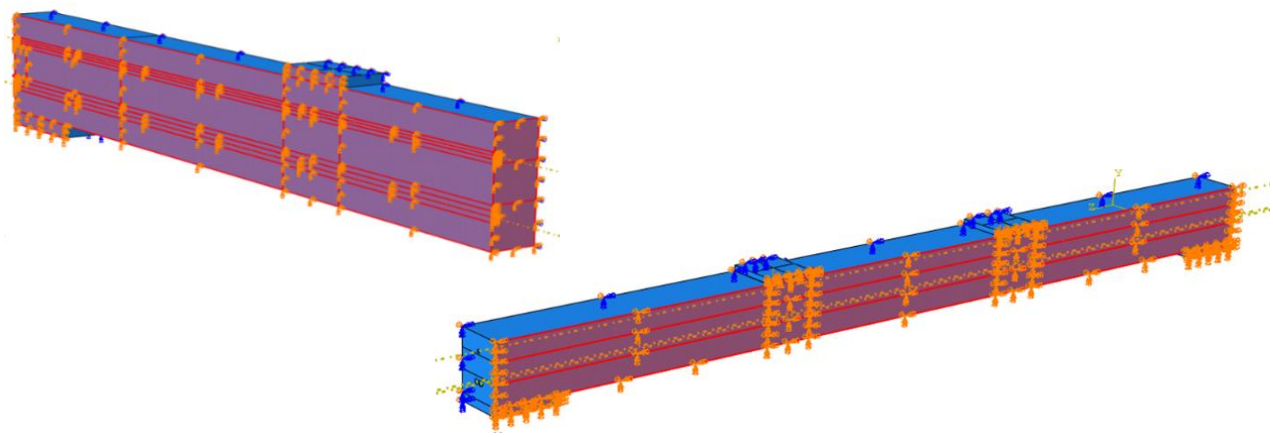

Figure 5 - Boundary conditions considered in the slabs with continuous reinforcement (top) and in the slabs with mid-span lap splices (bottom)

4. Numerical results and discussion

4.1 Mechanical analysis

Figure 6 to Figure 8 present the load vs. mid-span displacement curves obtained from the numerical models (for both approaches in terms of bond properties) plotted against the experimental results obtained in [10]. The results obtained numerically show a reasonable (GFRP reinforced slabs) to good (steel reinforced slab) agreement with the experimental results.

The RC model (steel reinforced slab), Figure 6, presents a flexural failure mode with concrete crushing, consistent with the design. It is also possible to verify that the failure load calculated numerically shows good agreement with the failure load obtained experimentally (with a difference of about 4%). However, the model presents a slightly higher stiffness which can be explained by an eventual imprecision on the definition of the elastic modulus and fracture energy of concrete.

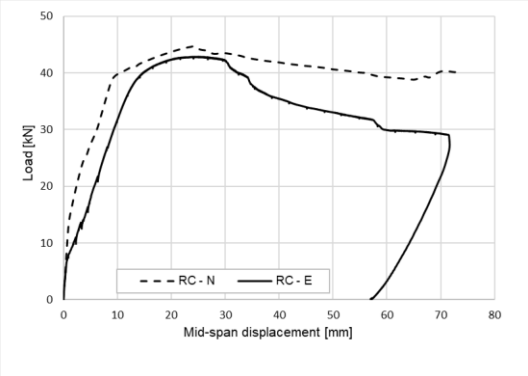

Figure 6 - Load-displacement curves for the RC slab: experimental (E) and numerical (N)

As in the RC model, the results obtained from the models of the slabs GFRP25 and GFRP35 show a reasonable agreement with the experimental results. Regarding the overall behaviour of the models it is possible to verify decreases of the load with the cracking of the concrete; these reductions can be explained by the lower elastic modulus of the GFRP rebars (when compared to that of the steel rebars) and by the slip of the rebars inside the concrete. However, it is important to mention that the reductions registered in the model with a bond between the rebars and the concrete described by a bond *vs*. slip law are considerably higher than those measured in the experimental tests. This can be explained by an eventual slight imprecision on the (experimental) definition of this law. Nonetheless, these reductions were also registered in the models that considered a perfect bond, so further explanations must be pursued, such as the eventual consideration of more flexible support conditions in the models than in the tests (where some friction may have occurred). Regarding the elastic stiffness and overall resistance, the models of the GFRP25 and GFRP35 slabs present higher values than those obtained in the tests, Figure 7; particularly, the failure loads calculated numerically present differences of about 22% and 32%, respectively, in the models GFRP25 and GFRP35.

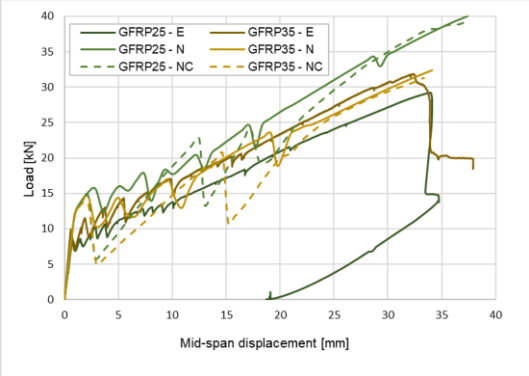

Figure 7 - Load-displacement curves for the GFRP25 and GFRP25 slabs: experimental (E), numerical (N) and numerical with bond-slip law (NC)

This can be explained by a slight imprecision on the definition of the material properties, particularly, the transverse elastic modulus of the GFRP rebars (which was considered equal to the longitudinal elastic modulus) and the compressive strength of the concrete.

Figure 8 presents the load *vs*. mid-span displacement curves obtained numerically for the slabs with mid-span lap splices plotted against the results obtained in the experimental tests.

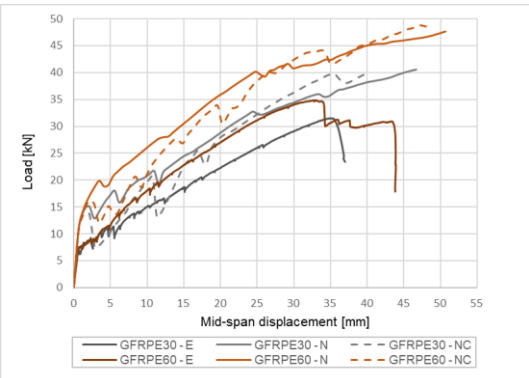

Figure 8 - Load-displacement curves for the GFRPE30 and GFRPE60 slabs: experimental (E), numerical (N) and numerical with bond-slip law (NC)

As in the GFRP25 and GFRP35 models, the numerical results for the GFRPE30 and GFRPE60 slabs show reductions of the force with the cracking of the concrete and slightly higher resistance and stiffness than the slabs tested experimentally. Notwithstanding the existence of mid-span lap splices, GFRPE30 and GFRPE60 models present higher failure loads than the correspondent slab with

continuous reinforcement (GFRP25) – this result is consistent with the experimental result and suggests that, at room temperature, the existence of a mid-span reinforcement might be a more determining factor than the possible slip of the rebars. Accordingly, the consideration of a higher lap splice length increases the failure load, as expected and as observed in the tests.

The GFRP reinforced slabs present patterns of plastic deformations in concrete consistent with a shear failure mode (as shown in Figure 9 for the GFRP25-NC model), even though they were designed (analytically) to present a flexural failure mode with concrete crushing – these failure modes

The numerical results show a good agreement with the experimental results. These results are obtained from the nodes of the mesh elements considered so that the results depend on the discretization of the mesh; therefore, it is not possible to guarantee readings at the exact location where the thermocouples were placed. However, it is to be expected that with a sufficiently refined mesh (as it is the case) the curves will show good agreements.

The results obtained from the rebars show the highest deviations when compared to the experimental results. This may be explained by a slight uncertainty on the positioning of the thermocouples (in the numerical models the

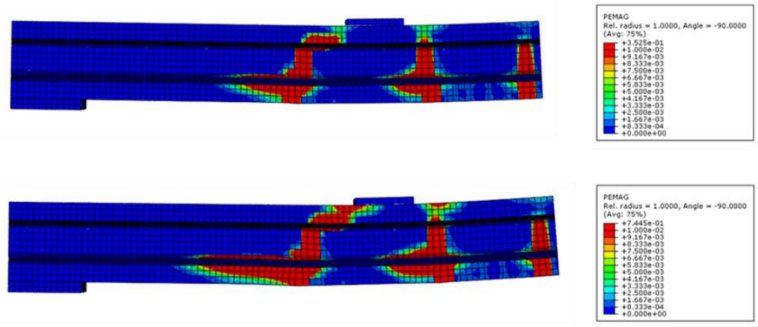

Figure 9 - Evolution of plastic deformations associated with shear failure of the GFRP25 slab - formation of shear concrete crack

are consistent with those observed experimentally for all slabs, with the exception of the GFRPE30 slab, which presented a failure mode due to the mid-span slip of the GFRP rebars. This difference between the expected behaviour and that experimentally and numerically observed may be explained by: (i) some uncertainty regarding the material properties, (ii) a slight overestimation of the shear resistant capacity of the slabs, namely of the transversal resistance of the rebars; and (iii) the small gap in shear design (in fact, the shear failure load was merely 9% and 20% higher than that corresponding to the flexural failure mode, respectively, in the GFRP25 and GFRP35 slabs [10].

4.2 Thermal analysis

Figure 10 to Figure 12 show the results of the thermal analysis by comparing the results obtained experimentally by Santos [10], during the fire resistance tests, with the numerical results, in different relevant points of the five slab strips, namely the lower and upper surface of the slab strips and the rebars, mid-span. The thermocouples T7 of the GFRP35 slab and T10 of the GFRPE30 slab did not provide accurate readings; accordingly, only the results of the thermocouple T7 (GFRP35) are shown to illustrate the anomalous behaviour of that sensor.

temperatures were calculated at mid height of the rebars; in the tests, the thermocouples were placed in that position prior to concreting but that operation together with the vibration of concrete may have caused a deviation on the position).

In the experimental tests, the slabs were subjected to a mechanical load (for a fire combination) which explains the premature failure of the slabs with lap splices, GFRPE30 and GFRPE60, before the end of the 2 hours; effectively, these slabs present drastic reductions of the fire exposure time and, in consequence, quite lower maximum temperatures in the nodes by the end of the tests.

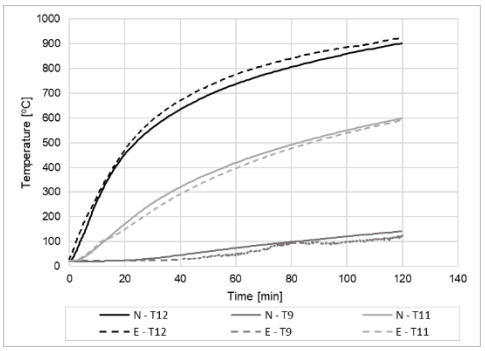

Figure 10 – Evolution in the nodal temperatures of the RC slab: experimental (E) and numerical (N)

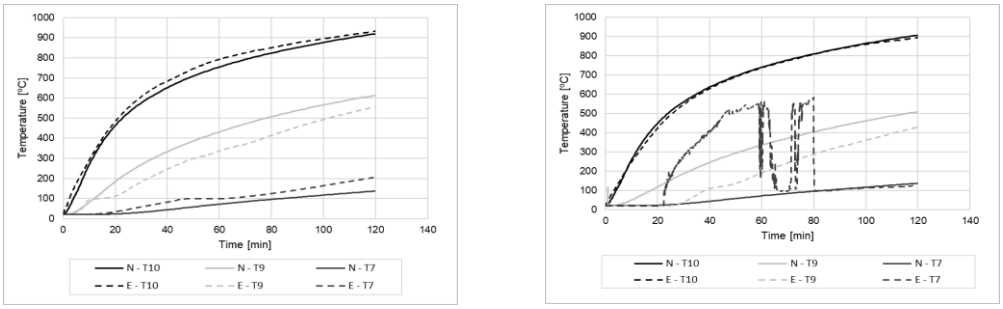

Figure 11 - Evolution in the nodal temperatures of the GFRP25 (left) and GFRP35 (right) slabs: experimental (E) and numerical (N)

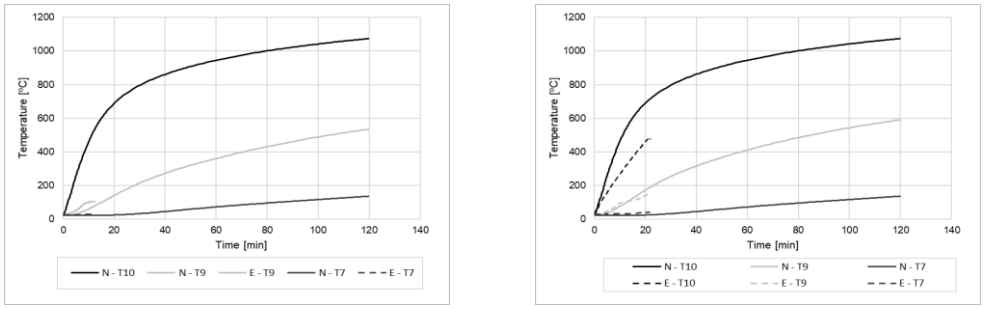

Figure 12 - Evolution in the nodal temperatures of the GFRPE30 (left) and GFRPE60 (right) slabs: experimental (E) and numerical (N)

4.3 Thermo-mechanical analysis

As mentioned, the fire behaviour of the slabs was assessed, by combining a mechanical load (corresponding to a fire combination) with the temperatures attained in the thermal analysis.

Figure 13 presents the evolution of the variation of mid-span displacement with time for the RC slab (steel reinforcement) plotted against the experimental results. The numerical displacements are higher than the experimental results with a difference at 116 minutes of 12 mm (40 mm and 28 mm, respectively in the numerical model and in the test); the experimental test was stopped at 116 minutes without occurrence of slab failure, which is consistent with the 120 minutes attained in the numerical model.

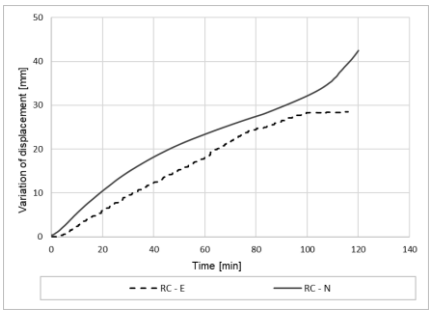

Figure 13 –Experimental (E) and numerical (N) evolution of the mid-span displacement in the RC slab

Figure 14 presents the evolution of the mid-span displacement with time for the GFRP25 and GFRP35 slabs (GFRP continuous reinforcement) plotted against the experimental results for both slabs. The numerical variation of the displacements is higher than the experimental variation, for both approaches concerning the rebar-concrete interaction. The numerical models present a steeper evolution of the displacements up to until 20 minutes, which may be explained by the uncertainty about some material properties, as the elastic modulus of concrete and the rebars and the bond between both materials. The numerical models of the GFRP25 slab were stopped before 120 minutes (due to non-convergence), whereas the GFRP35 models reached the end of the test without failure occurrence.

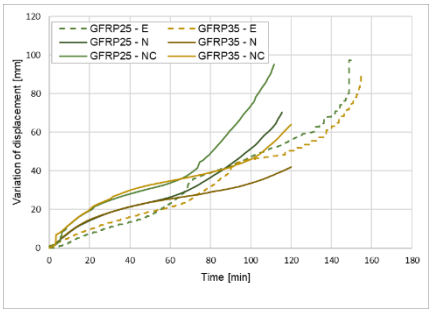

Figure 14 - Experimental (E), numerical (N) and numerical with bond-slip law (NC) evolution of the mid-span displacement in the GFRP25 and GFRP35 slabs

Figure 15 presents the evolution of the numerical normalized stress on the upper and lower nodes of

the reinforcing rebars, that is, the ratio between the calculated stress in a node for a given instant and the (theoretical) strength at that time/temperature, for the GFRP25 and GFRP35 models. The lower fibres of the rebars attain their maximum resistance at 90 and 120 minutes, respectively, in the GFRP25 and GFRP35 models; however, at these instants the upper fibres still show a reserve of tensile strength. Furthermore, the bond between the rebars and the concrete is assured after the rebars attain 140ºC (temperature at which the bond was specified to be null) in both slabs. This may be explained by a possible "cable effect" (assured by the colder anchorages of the rebar), which guarantees the structural integrity of the slabs.

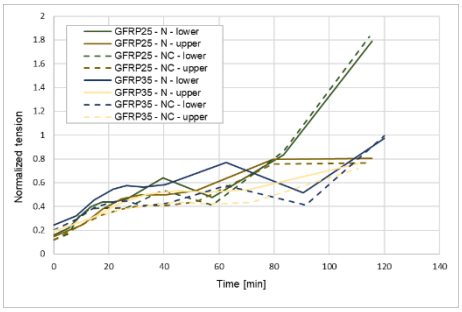

Figure 15 – Numerical evolution of the normalized stress in the rebars (lower and upper fibres) of the GFRP25 and GFRP35 slabs: numerical (N) and numerical with bond-slip law (NC)

Regarding the slabs with lap splices, Figure 16 shows that both numerical models with the bond described by a bond-slip law were able to reproduce the failure of the elements; both slabs presented failure after about 20 minutes, regardless of the splice length. These results suggest that the GFRPE60-NC model was not capable of reproducing the effects of increasing this length and that, for slabs with lap spliced reinforcement, the behaviour of the element is strictly a function of the temperatures attained in the rebars (which are dependent of the concrete cover).

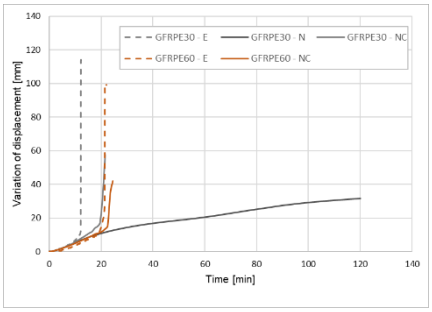

Figure 16 - Experimental (E), numerical (N) and numerical with bond-slip law (NC) evolution of the mid-span displacement in the GFRPE30 and GFRPE60 slabs

Figure 17 shows the evolution of the shear stress between the rebars and the concrete for the GFRPE60-NC model, in the upper and lower fibres of the rebar (the GFRPE30-NC curve is similar). The analysis of the curve shows that the complete loss of bond between the concrete and the rebars is attained at 22.5 minutes; at about 17.5 minutes, the upper fibres reach the glass transition temperature (about 100ºC) and the lower fibres are at about 200ºC.

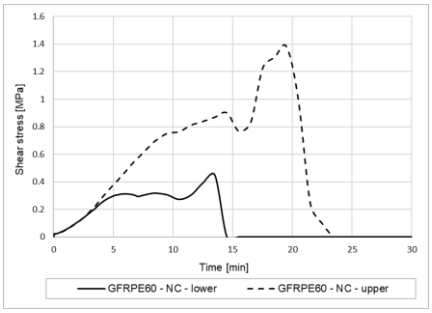

Figure 17 – Evolution of the shear stress in the rebars of the GFRPE60-NC slab (upper and lower)

5. Conclusions

The present numerical investigation aimed at studying the behaviour of GFRP-RC slab strips subjected to fire and evaluating the effects of two different approaches for simulating the bond between the concrete and the rebars. From the results obtained the following main conclusions can be drawn:

1. At ambient temperature, the existence of a mid-span reinforcement (through the consideration of lap splices) may be a more determining factor than the possible slip of the rebars.
2. The consideration of a temperature dependent bond shows greater significance when applied to GFRP-RC slabs with lap spliced rebars, precisely due to the slipping failure of the rebars.
3. For the slab geometry and conditions used in this study, increasing the concrete cover by 10 mm can increase the fire resistance by about 30 minutes.
4. The models of the slabs with lap splices were not capable of accurately reproducing the effects of increasing the splice length.
5. The numerical analysis confirmed that GFRP-RC slabs with continuous reinforcement exhibit substantial fire resistances (about 120 minutes) provided that the anchorage zones of the rebars remain comparably cold and that the presence of lap splices directly exposed to heat significantly decreases the fire resistance to about 20 minutes.
6. The bond *vs*. slip relations that were used to simulate the bond between the rebars and concrete may have slightly overestimated the bond performance.

6. References

[1] L. Bank, Composites for Construction: Structural Design with FRP Materials, USA: John Wiley & Sons, 2006.

[2] M. Rafi and A. Nadjai, “Numerical modelling of carbon fibre-reinforced polymer and hybrid reinforced concrete beams in fire”, *Fire and Materials, Vol.37, No.5,* pp. 374-390, 2013.

[3] M. Rafi and A. Nadjai, “Parametric finite element analysis of FRP reinforced concrete beams in fire and design guidelines”, *Fire and Materials, Vol.38, No.3,* pp. 293-311, 2014.

[4] M. Rafi and A. Nadjai, “Fire tests of hybrid and CFRP bar reinforced concrete beams”, *ACIMaterials Journal, Vol.8, No.3,* pp. 252-260, 2011.

[5] British Standards Institution, *Code of Practice for Structure Use of Concrete, CP110,* London, 1972.

[6] NP EN, 1992-1-2, *Projecto de estruturas de betão, Parte 1-2: Regras gerais, Verificação de resistência ao fogo,* Lisboa: IPQ, 2010.

[7] B. Yu and V. Kodur, “Evaluating fire Response of Concrete Beam Reinforced with FRP Rebars”, em *7th International Conference on Structures in Fire*, 2012.

[8] B. Yu and V. Kodur, “Factors governing the fire response of concrete beams reinforced with FRP rebars”, *Composite Structures, Vol.100,* pp. 257-269, 2013.

[9] E. Nigro, G. Cefarelli, A. Bilotta, G. Manfredi and E. Cosenza, “Comparison between results of numerical simulations and experimental tests on FRP RC slabs in fire situation”, em *7th International Conference on Structures in Fire*, Zurich, Switzerland, 2012.

[10] P. Santos, “Resistência ao fogo de elementos de betão reforçados com varões em compósito de GFRP,” Dissertação para a obtenção do grau de mestre em Engenharia Civil, IST, 2016.

[11] J. Lee and G. Fenves, “Plastic-damage model for cyclic loading of concrete structures”, *Journal of Engineering Mechanics, ASCE, Vol.124,* pp. 892-900, 1998.

[12] H. Hilsdorf and W. Brameshuber, “Code-type formulation of fracture mechanics concepts for concrete”, *International Journal of Fracture, Vol.51, No.1,* pp. 61-72, 1991.

[13] J. Sampaio, J. Alfaiate, C. Tiago and J. Correia, “Task 5: Simulation of Thermal Behaviour and Preliminary Simulation of Mechanical Behaviour”, FCT project PTDC/ECM/118271/2010, “Fire protection of reinforced concrete structural elements strengthened with carbon fibre reinforced polymer (CFRP) systems”, Task 5, Report ICIST DTC 05/2014, 2014.

[14] Y. C. Wang, P. M. H. Wong and V. Kodur, “An experimental study of the mechanical properties of fibre reinforced polymer (FRP) and steel reinforcing bars at elevated temperatures”, *Composite Structures Vol.80,* pp. 131-140, 2007.

[15] Y. Bai, T. Vallée and T. Keller, “Modeling of thermo-physical properties for FRP composites under elevated and high temperature”, *Composites Science and Technology, Vol. 67,* pp. 3098-3109, 2007.

[16] I. Rosa, L. Granadeiro, J. Firmo, J. Correia and A. Azevedo, “Effect of elevated temperatures on the bond behaviour of GFRP bars to concrete – Pull-out tests”, em *3rd International Conference on Protection of Historical Constructions*, Lisbon, Portugal, 2017.